TECHNICAL ARTICLE

An investigation into the temperature phase transitions of synthesized materials with Al- and Mg-doped lithium manganese oxide spinels by *in situ* powder X-ray diffraction

C. D. Snyders,[1,a] E. E. Ferg,[1] and D. Billing[2]
[1]*Department of Chemistry, Nelson Mandela Metropolitan University, P.O. Box 77000, Port Elizabeth 6031, South Africa*
[2]*School of Chemistry, University of the Witwatersrand, Private Bag 3, Johannesburg 2000, South Africa*

(Received 18 May 2016; accepted 23 October 2016)

Three spinel materials were prepared and characterized by *in situ* powder X-ray diffraction (PXRD) techniques to track their phase changes that occurred in the typical batch synthesis process from a sol–gel mixture to the final crystalline spinel oxide. The materials were also characterized by thermal gravimetric analysis, whereby the materials decomposition mechanisms that were observed as the precursor, was gradually heated to the final oxide. The results showed that all the materials achieved their total weight loss at about 400 °C. The *in situ* PXRD analysis showed the progression of the phase transitions where certain of the materials changed from a crystalline precursor to an amorphous intermediate phase and finally to the spinel cathode oxide ($Li_{1.03}Mg_{0.2}Mn_{1.77}O_4$). For other materials, the precursor would start as an amorphous phase and upon heating, convert into an impure intermediate phase (Mn_2O_3) before forming the final spinel oxide ($Li_{1.03}Mn_{1.97}O_4$). On the other hand, the $LiAl_{0.4}Mn_{1.6}O_4$ would start with an amorphous precursor, with no intermediate phases and immediately formed the final spinel oxide phase. The *in situ* PXRD study also showed the increases in the materials respective lattice parameters of the crystalline unit cells upon heating and the significant increases in their crystallite sizes when heated above 600 °C. © *2016 International Centre for Diffraction Data*. [doi:10.1017/S088571561600066X]

Key words: *in-situ* powder X-ray diffraction, Al- and Mg-doped $LiMn_2O_4$, lattice parameter, amorphous and crystalline precursors, intermediate Mn_2O_3

I. INTRODUCTION

Lithium manganese oxide occurs in various forms, whereby the three-dimensional (3D) structure of the spinel, $LiMn_2O_4$, is one of the common materials used in lithium-ion cells (Thackeray *et al.*, 1984; Ohzuku *et al.*, 1990; Rossouw *et al.*, 1990; Arora *et al.*, 1998; Wang *et al.*, 2012). In the spinel ($LiMn_2O_4$) structure, lithium is located at the tetrahedral 8a sites, manganese at the octahedral 16d sites, and oxygen on the 32e cubic close packing sites. The Jahn–Teller effect occurs because of the coexistence of Mn^{3+} and Mn^{4+} in the $LiMn_2O_4$ structure where the Mn^{3+} concentration is slightly higher than that of Mn^{4+}. As the Mn^{3+} concentration increases the distortion effect that becomes even more noticeable, causes a breakdown in the crystal lattice during capacity cycling (Gummow *et al.*, 1994; Manev *et al.*, 1995; Yamada, 1996; Li *et al.*, 2009). Hence, upon repeated capacity cycling at elevated temperatures, this material suffers from relatively fast capacity fading that prevents it from wider commercial use. This capacity fading is normally observed around the 3 V region where the Jahn–Teller distortion effect starts to occur near the surfaces of the spinel material's structure (Gummow *et al.*, 1994). Also, the Mn slightly dissolves into the electrolyte causing further electrolyte decomposition (Gummow *et al.*, 1994; Jang *et al.*, 1996). In these materials, the capacity fading during cycling was reduced by doping with various metals (such as Mg, Fe, Al, Cr, Ni, Co, or Ti) (Guohua *et al.*, 1996; Hernán *et al.*, 1999; Sun *et al.*, 1999; Thirunakaran *et al.*, 2008; Huang *et al.*, 2012), adjusting the lithium content or concentration (Thackeray *et al.*, 1983, 1984, 1992; Tarascon and Guyomard, 1991, 1993) or by coating the spinel material with various materials (such as carbons, other transition metal oxides, or doped spinel oxides) (Lee *et al.*, 2004; Chung *et al.*, 2005; Li *et al.*, 2006).

The cathode's active materials for lithium-ion cells are prepared by various synthesis methods such as combustion, hydrothermal, emulsion, microwave, pechini, co-precipitation, solid-state, sol–gel, and spray pyrolysis methods (Sun *et al.*, 1999; Li *et al.*, 2000; Wu and Chen, 2003; Jugovic and Uskokovic, 2009; Palomares *et al.*, 2012). Recent developments in these synthesis methods have remarkably improved the materials' electrochemical performance such as cycle life and capacity and to make them more cost-effective and uniform in their material's morphology. Traditionally, the most common method of synthesis was the solid-state technique, whereby the active material was obtained by mixing or grinding the right proportions of various solid materials together and applying high temperatures over longer periods of time (Ohzuku *et al.*, 1990; Zhong *et al.*, 1997; Sun *et al.*, 1999; Lui *et al.*, 2013). More recently, other methods involved in the formation of sol–gel materials as precursors, require considerably less time and energy (Hwang *et al.*, 2001a, 2001b; Fu *et al.*, 2005; Lui *et al.*, 2013).

It is of importance that the materials are accurately prepared and their phase transitions understood during the

[a]Author to whom correspondence should be addressed. Electronic mail: Charmelle.Snyders@nmmu.ac.za

heating process. These observations can be carefully studied by *in situ* powder X-ray diffraction (PXRD). This study investigated the phase changes of the undoped ($Li_{1.03}Mn_{1.97}O_4$) together with two doped materials ($LiM_xMn_{2-x}O_4$, M = Mg, Al) that were prepared by the sol–gel method by heating them from room temperature to 850 °C, the temperature that was most commonly reported in the literature to form the final oxide (Sun, 1997; Lee *et al.*, 1998; Hwang *et al.*, 2001a, 2001b).

An important parameter that could be determined from powder diffraction patterns was the materials crystallite size. For many years, the Scherrer equation was used to determine the average crystal or crystallite size distribution of a powdered material by considering the diffraction peak width at half-maximum intensity (Kim *et al.*, 2001; Meier, 2004; Rehani, *et al.*, 2006; Yi *et al.*, 2006a, 2006b). However, the contribution to the diffraction peak width can result from a number of factors besides the crystallite size parameter and it is common practice to consider a number of peaks in a well-defined diffraction pattern to obtain an average value for the contribution of the crystallite size to the peak shape. With the use of full pattern Rietveld refinement and the fundamental parameter approach to both quantification of phases and the qualification of the various contributions to the peak and diffraction pattern shape, it has become common practice to define the crystallite size parameter that was obtained from the refinement of the whole pattern within typical Rietveld refinement software such as Topas® (Bruker, 2009). In this study the materials' unit-cell lattice parameter (a) and the crystallite size parameter (LVol-IB) of the obtained diffraction patterns was allowed to refine and compared over the temperature range of the *in situ* PXRD study.

II. EXPERIMENTAL

The spinel precursor materials together with some variations in the doped materials (Al and Mg) were synthesized by the conventional sol–gel method described by a number of authors (Sun *et al.*, 1997; Liu *et al.*, 2004; Fu *et al.*, 2005; Thirunakaran *et al.*, 2008). The method used in this study involved the dissolving of manganese, lithium, magnesium and/or aluminium salts (acetates) in the right stoichiometric amounts to make up the $Li_{1.03}Mn_{1.97}O_4$, $LiAl_{0.4}Mn_{1.6}O_4$, and $LiMg_{0.2}Mn_{1.77}O_4$, respectively. The carrier lignin used was citric acid (1 molar ratio of acid to metal ion) dissolved in distilled water, which then formed an aqueous solution. This aqueous solution was then heated to 120 °C with continuous stirring until the gel-solid precipitate was formed. Further heating without stirring was required resulting in the solid powder precursor, which was then completely dried in a drying oven at 140 °C for about 5 h. The stoichiometric amounts, $Li_{1.03}Mn_{1.97}O_4$, were used because according to Singh *et al.* (2010) these ratios still retained the same structure as $LiMn_2O_4$ and showed stable electrochemical performances. Phase identification of the various precursors was done by PXRD at room temperature on a Bruker D2 powder X-ray diffractometer using Cu radiation with a Lynxeye detector. A scan range of 5°–70° was used for all precursor PXRD analyses. All room temperature phase analysis was done on this instrument. The *in-situ* temperature PXRD was done on a Bruker D8 Advance consisting of a Vantec detector and a Cu radiation source with a Goebel mirror. The cell used for this particular instrument was an Anton Parr XRK900 consisting of a macor sample holder with a Pt foil insert. The *in situ* PXRD analysis consisted of placing the precursor sample into a ceramic sample stage, which was enclosed in the heating stage, whereby the precursor was gradually heated to the materials' final oxide phase under an air atmosphere from 30 to 850 °C at 6 °C min^{-1} and cooling it immediately to room temperature again followed by a final PXRD scan of the sample. A scan range of 5°–70° was used for all *in situ* PXRD analysis, collecting a full PXRD pattern (also referred to as variable temperature, VT-scans) at every 50 °C intervals (after room temperature scan). Phase quantification for the various PXRD patterns was done by Rietveld refinement, allowing the respective lattice parameter (a) and the crystallite size parameter (LVol-IB) to refine (additional Rietveld refinement parameter results, such as R_{wp} and GoF, are provided in the supplementary information). Within the Topas® refinement software, the site occupancy of the Mn-ion and the respective doped-ions were set at the ratio $1-x$ and x, respectively, where x would be the mole amount of the doped species in the sample.

Thermogravimetric analysis (TGA) was done on a SDT Q600 (TA Instruments) and quantification of the various phases was analyzed using TA Universal Analysis v4.5A software. The analysis heating rate was from 25 to 800 °C at 1 °C min^{-1} under an air atmosphere.

Brunauer–Emmett–Teller (BET) analysis was done on a Micromeritics Gemini 2375 instrument and quantification of the various oxides was done using StarDriver v2.03 software. Samples were degassed for 1 h under nitrogen at 300 °C.

III. RESULTS AND DISCUSSION

The overlayed curves of the TGA for the three synthesized materials are shown in Figure 1. In general, the results showed a first decomposition step or weight loss between 200 and 300 °C, this weight loss could be related to the water loss that was possibly trapped within the precursor powder. The results also showed that the doped oxide materials produced multiple weight loss, whereas the undoped oxide material obtained a single weight decomposition. The TGA curves for Mg and Al-doped spinel materials showed complete decomposition at higher temperatures (approximately 375 and 325 °C, respectively) when compared with the undoped spinel

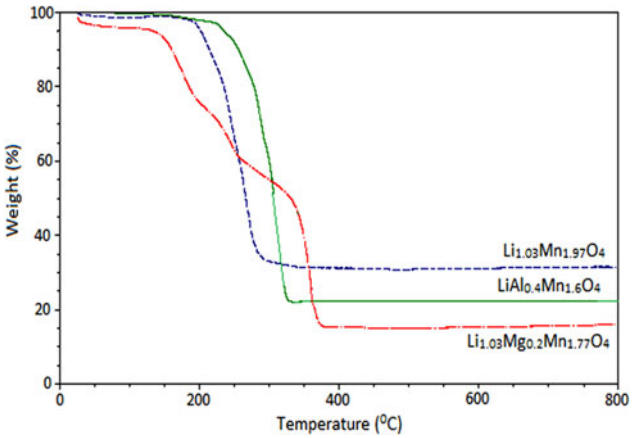

Figure 1. (Color online) TGA curves of $Li_{1.03}Mn_{1.97}O_4$, $Li_{1.03}Mg_{0.2}Mn_{1.77}O_4$, and $LiAl_{0.4}Mn_{1.6}O_4$.

https://doi.org/10.1017/S088571561600066X Published online by Cambridge University Press

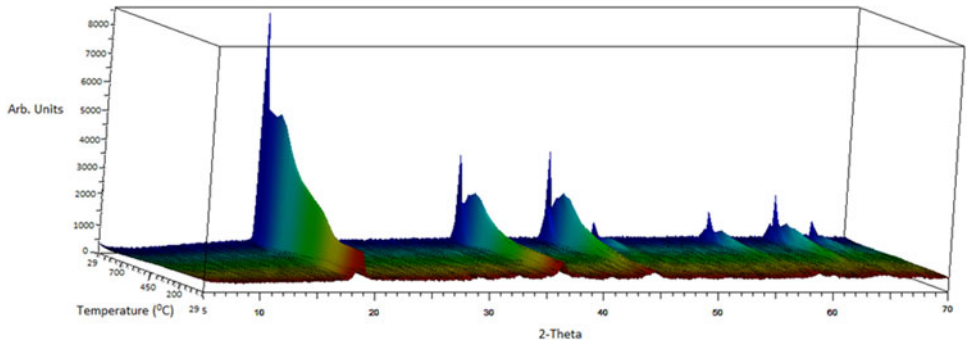

Figure 2. (Color online) *In-situ* PXRD VT-scan of $Li_{1.03}Mn_{1.97}O_4$ made from the precursor. The temperature scale is shown in arbitary units.

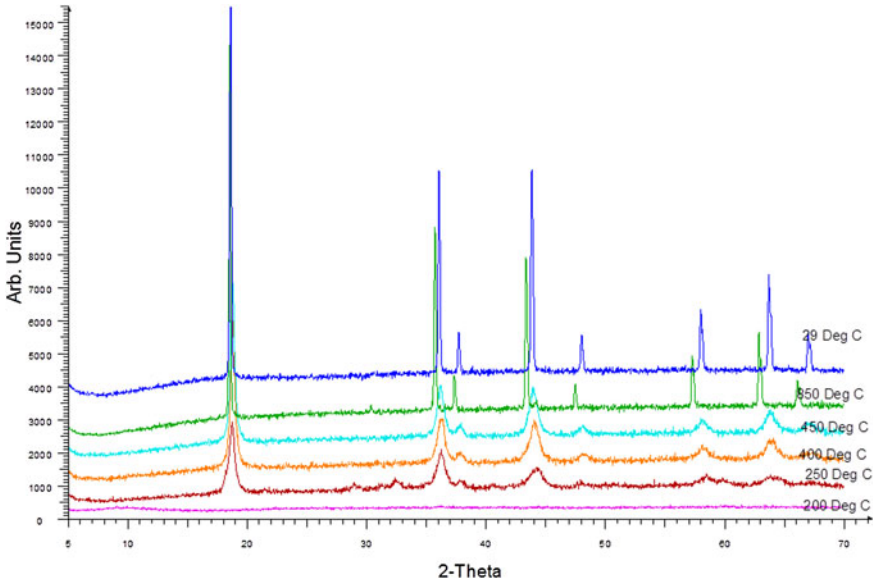

Figure 3. (Color online) Staggered PXRD patterns of $Li_{1.03}Mn_{1.97}O_4$ at specfic temperatures of interest from the *in situ* set of results.

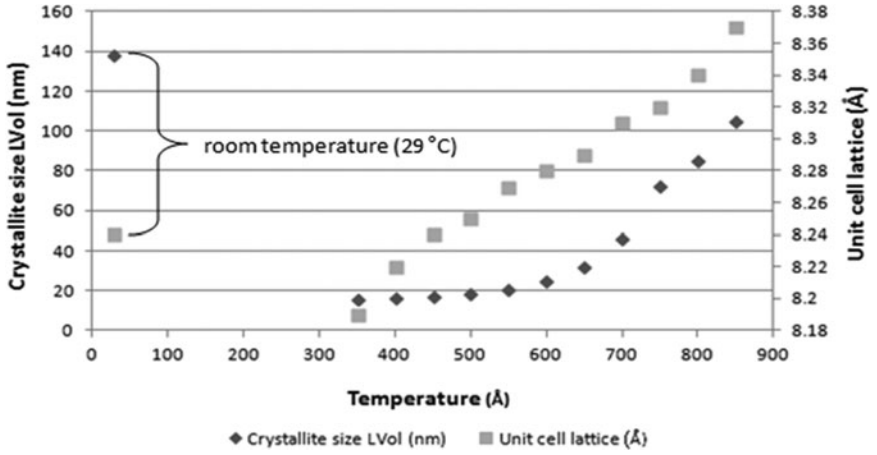

Figure 4. Graphical display of *in situ* $Li_{1.03}Mn_{1.97}O_4$ Rietveld results.

$LiMn_2O_4$ (at approximately 280 °C), concluding that these doped materials formed its final oxide later than the undoped oxide. At 400 °C the TG analysis obtained no further weight decomposition concluding final phase formation, which was supported by these *in situ* results (Figures 2–10).

The *in situ* PXRD 3D graph over the temperature range from 25 to 850 °C is shown in Figure 2. A number of selected diffraction patterns at certain temperatures are shown in Figure 3.

The results showed that the precursor material was amorphous at room temperature up to about 200 °C. At 250 °C the formation of a crystalline intermediate phase was observed to form up to about 350 °C, which could relate to Mn_2O_3 (Lee *et al.*, 1998; Hwang *et al.*, 2001a, 2001b; Wang *et al.*, 2003;

https://doi.org/10.1017/S088571561600066X Published online by Cambridge University Press

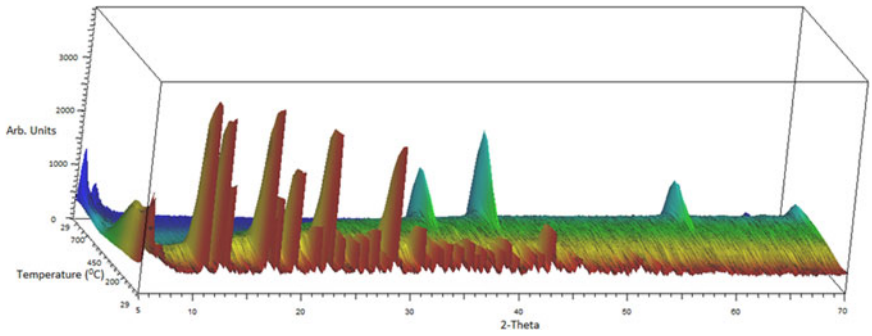

Figure 5. (Color online) *In-situ* PXRD VT-scan of $Li_{1.03}Mg_{0.2}Mn_{1.77}O_4$ made from the precursor. The temperature scale is shown in arbitary units.

Seyedahmadian *et al.*, 2013). The PXRD analysis also observed very broad peaks at this temperature (250 °C), which could be an indication of a low crystallinity material or a material of nanoscale particles. At 400 °C the formation of the typical spinel crystalline phase ($Li_{1.03}Mn_{1.97}O_4$) was seen to form with the respective diffraction peaks being still relatively broad up to about 600 °C. As the temperature increased up to 850 °C, the diffraction peaks became significantly sharper, implying a growth in the crystallite size. The changes in the crystal unit-cell parameter (*a*) and the crystallite size (LVol-IB) from 350 to 850 °C are shown in Figure 4. For comparison purposes, the unit-cell parameter and crystallite size of the material that was allowed to cool to room temperature are also shown.

The results showed that there was a noticable linear increase in unit-cell lattice expansion of about 0.32×10^{-3} Å $°C^{-1}$ as the temperature increased from 300 to 850 °C similar to studies reported by Sun *et al.* (1997). When the sample was cooled back to room temperature, the unit-cell lattice decreased to 8.24 Å, which was in agreement to studies reported by Singh *et al.* (2010), Sun *et al.* (1997), and Lee *et al.* (1998). The resutls also showed that the materials' crystallite size started to increase signficantly at about 600 °C. Over the temperture range of up to 850 °C, there would be almost a 323% increase in the crystallite size that was based on the LVol-IB (nm) parameter determined calculation from Rietveld refinement. This related to about 0.34 nm $°C^{-1}$ change in crystallite size. When the sample was allowed to cool to room temperature from 850 °C, the crystallites continued to grow, where the room temperature sample showed a crystallite size of 137.8 nm, which was a further growth of about 31% in crystallite size.

The *in situ* variable temperature PXRD scan of the precursor material as it changed with temperature to form the final $Li_{1.03}Mg_{0.2}Mn_{1.77}O_4$ is shown in Figure 5. Selected diffraction patterns of interest at certain temperatures are shown in a staggered format in Figure 6.

The results showed that the precursor material was crystalline at room temperature up to about 200 °C. At about 250 °C the material's crystalline structure collapsed to form an amorphous intermediate phase up to about 300 °C. This was in agreement with the TGA curves (Figure 1) that showed a significant mass loss to occur between 250 and 300 °C. At about 350 °C the amorphous phase collapsed and the formation of a mix amorphous-final crystalline phase was observed, before the formation of the typical spinel crystalline phase ($Li_{1.03}Mg_{0.2}Mn_{1.77}O_4$) was seen to start forming at about 400 °C. As the temperature increased to 850 °C, the diffraction peaks became significantly sharper and more defined, implying a growth in the crystallite size of the material. The changes in the crystal unit-cell parameter (*a*) and the crystallite size (LVol-IB) from 350 to 850 °C are shown in Figure 7. For comparison purposes, the unit-cell parameter and crystallite size at room temperature are also shown.

The results showed that there was a noticeable increase in the unit-cell lattice expansion of about 0.27×10^{-3} Å $°C^{-1}$ as

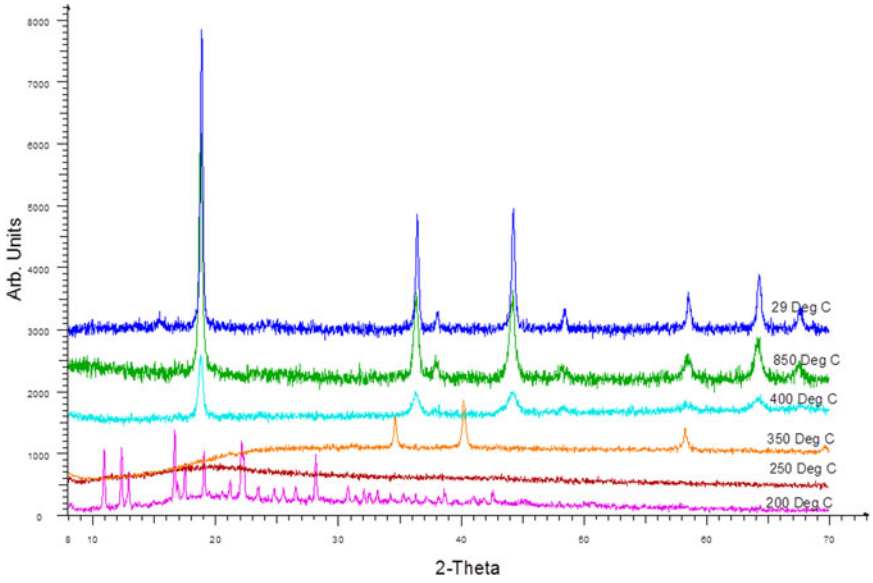

Figure 6. (Color online) Staggered PXRD patterns of $Li_{1.03}Mg_{0.2}Mn_{1.77}O_4$ at specfic temperatures of interest from the *in situ* set of results.

https://doi.org/10.1017/S088571561600066X Published online by Cambridge University Press

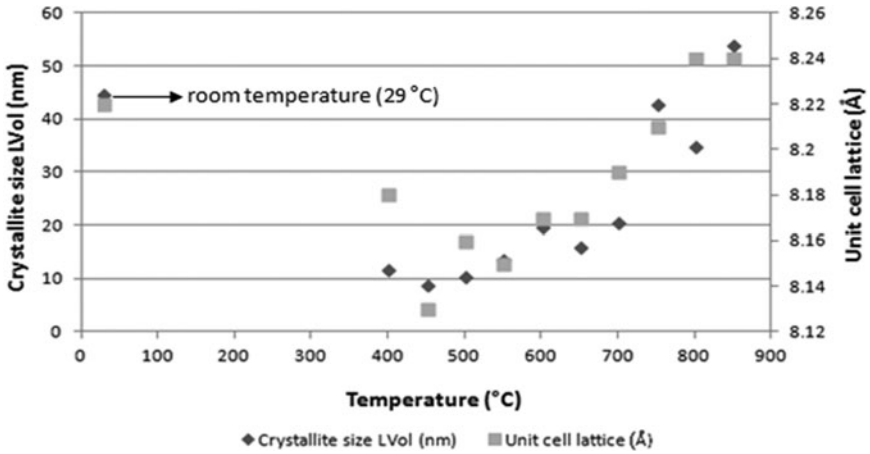

Figure 7. Graphical display of *in-situ* $Li_{1.03}Mg_{0.2}Mn_{1.77}O_4$ Rietveld results.

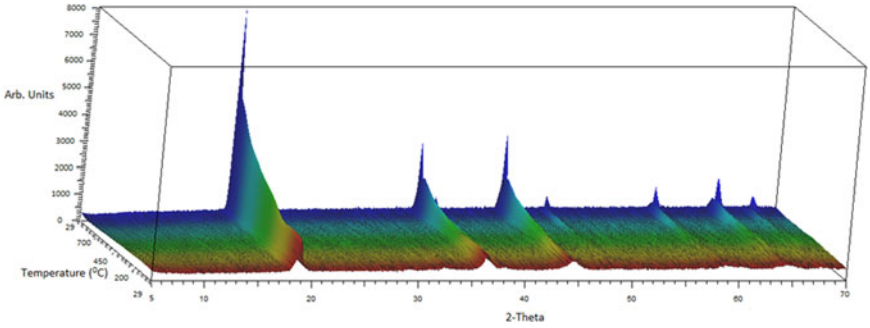

Figure 8. (Color online) *In-situ* PXRD VT-scan of $LiAl_{0.4}Mn_{1.6}O_4$ made from the precursor. The temperature scale is shown in arbitary units.

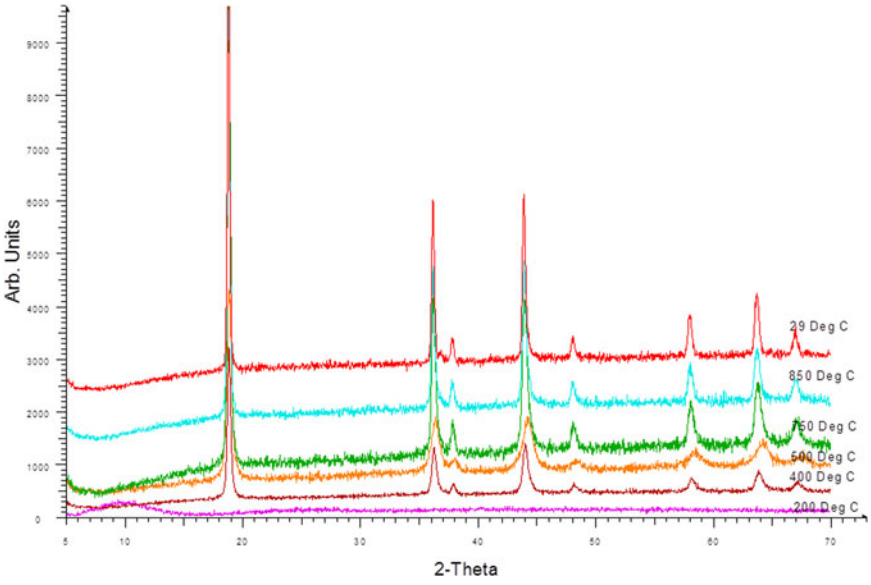

Figure 9. (Color online) Staggered PXRD patterns of $LiAl_{0.4}Mn_{1.6}O_4$ at specfic temperatures of interest from the *in-situ* set of results.

the temperature increased from 450 to 850 °C. When the sample was cooled back to room temperature, the unit-cell lattice decreased to 8.22 Å, which was in agreement with lattice parameters published for this type of material (Singh *et al.*, 2010). The crystallite size based on the full Rietveld refinement of the diffraction pattern showed a significant increase from about 550 °C, where there was about a 296% increase in the crystallite size from 550 to 850 °C based on the LVol-IB (nm) calculation. This related to about 0.15 nm $°C^{-1}$ change in crystallite size over that temperature range. When compared with the results of the previous sample, as the sample was allowed to cool to room temperature from 850 °C, the crystallite size did not change significantly (about 17%), which could be within experimental error.

The results showed that the doping of the managanese spinel with a small amount of Mg allowed for the material to

https://doi.org/10.1017/S088571561600066X Published online by Cambridge University Press

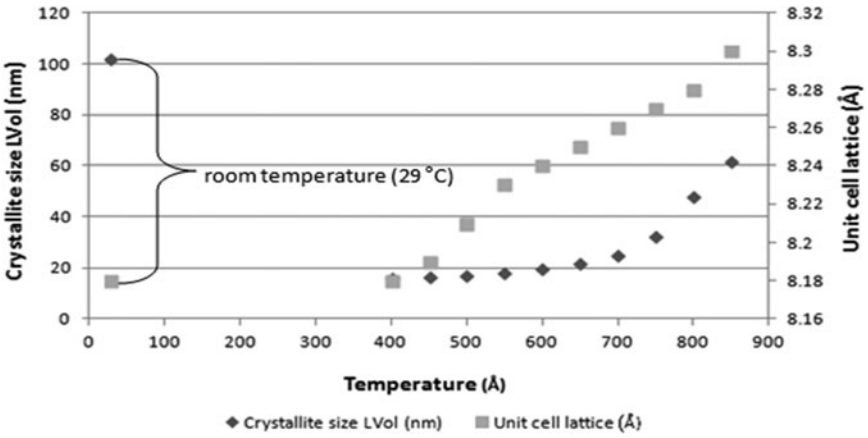

Figure 10. Graphical display of *in situ* $LiAl_{0.4}Mn_{1.6}O_4$ Rietveld results.

form the crystalline phase from an amorphous phase allowing for slightly smaller crystalites to grow at the higher temperatures. These results also correlated with the TGA curves (Figure 1) that showed multiple weight loss steps that can relate to the various phase changes (from precursor to final oxide) within these *in situ* PXRD results. At 400 °C the *in situ* PXRD results showed that the final spinel oxide was starting to form and that the TGA results showed no further weight loss to occur as the temperature continued to increase.

The *in situ* PXRD scan of the precursor material as it changed with temperature to form the final $LiAl_{0.4}Mn_{1.6}O_4$ is shown in Figure 8. Selected diffraction patterns of interest at certain temperatures are shown in a staggered format in Figure 9.

The results showed the precursor material was amorphous at room temperature up to about 350 °C. At 400 °C the formation of the typical spinel crystalline phase ($LiAl_{0.4}Mn_{1.6}O_4$) was seen to form with the diffraction peaks being relatively broad up to about 700 °C. As the temperature increased up to 750 °C, the diffraction peaks became significantly sharper, implying a growth in the crystallite size. The change in the crystal unit-cell parameter (*a*) and the crystallite size (LVol-IB) from 400 to 850 °C are shown in Figure 10. For comparison purposes, the unit-cell parameter and crystallite size at room temperature are also shown.

The results showed that there was a noticable linear increase in unit-cell lattice expansion of about 0.25×10^{-3} Å $°C^{-1}$ as the temperature increased from 400 to 850 °C. When the sample was cooled back to room temperature, the unit-cell lattice decreased to 8.18 Å and was similar (within negligible error range, 8.21 Å) to the unit-cell values reported in literature (Yi *et al.*, 2006a, 2006b; Kebede *et al.*, 2015). The crystallite size based on the full Rietveld refinement of the diffraction pattern started to increase signficantly from about 700 °C, where there was about 147% increase in the crystallite size from 700 to 850 °C based on the Lvol-IB (nm) calculation. This related to about 0.25 nm $°C^{-1}$ changes in crystallite size over that temperature range with the respective onset temperature in the change in crystallite size being slightly higher than the temperature observed for the other two materials reported. On cooling the sample back to room temperature, a similar increase in the crystallite size was observed to that of $Li_{1.03}Mn_{1.97}O_4$ (Figure 2) where the calculated Lvol-IB parameter at room temperature was 102 nm, a 65% increase when compared with the LVol-IB parameter at 850 °C.

The results showed that the doping of the lithium manganese oxide spinel with a small amount of Al allowed for the formation of smaller crystallites of around 20 nm up to the high temperature of 700 °C. These *in situ* PXRD results are in agreement with the TGA results (Figure 1) that showed complete formation of the final spinel oxide at around 350 °C with no further mass loss observed up to 800 °C.

In summary, the PXRD results and the characteristics of the three materials studied is shown in Table I.

The unit-cell lattice parameter, *a*, (Å) and crystallite size parameter, LVol-IB, (nm) of the doped spinel materials were comparatively slightly smaller at room temperature and 850 °C (Table I) and also at 600 °C (Table II) when compared with the undoped $Li_{1.03}Mn_{1.97}O_4$ spinel oxide material. This decrease would be because of the fact that the doped metals (Al and Mg) partially substituted Mn within the crystal unit cell of the spinel oxide. The change in the unit-cell lattice parameter when heated from 600 to 850 °C showed similar increases for the Mg and Al doped materials when compared with the undoped $Li_{1.03}Mn_{1.97}O_4$. A significant change was observed in the crystallite size, LVol-IB, of the various samples analysed upon heating from 600 to 850 °C. This study showed that upon heating to around 400 °C, all the spinel crystalline phase material would have formed for both

TABLE I. Summary of the spinel oxide materials *in situ* PXRD results.

Sample	$Li_{1.03}Mn_{1.97}O_4$	$LiAl_{0.4}Mn_{1.6}O_4$	$Li_{1.03}Mg_{0.2}Mn_{1.77}O_4$
Unit-cell lattice parameter at room temperature (Å)	8.24	8.18	8.22
Crystallite size parameter Lvol-IB at room temperature (nm)	137.8	102	44.7
Unit-cell lattice parameter at 850 °C (Å)	8.37	8.30	8.24
Crystallite size parameter Lvol-IB at 850 °C (nm)	104.8	62.0	53.9
Slope of the change in the unit-cell lattice with temperature from 600 to 850 °C (Å $°C^{-1}$)	0.32×10^{-3}	0.25×10^{-3}	0.27×10^{-3}
Slope on change in crystallite size (nm $°C^{-1}$)	0.34	0.25	0.15
% change in crystallite size from 600 to 850 °C	323	147	296

https://doi.org/10.1017/S088571561600066X Published online by Cambridge University Press

TABLE II. Summary of the spinel oxide materials crystallite and BET results at various temperatures.

	$Li_{1.03}Mn_{1.97}O_4$	$LiAl_{0.4}Mn_{1.6}O_4$	$Li_{1.03}Mg_{0.2}Mn_{1.77}O_4$
BET surface area at 800 °C ($m^2\ g^{-1}$)	5.48	18.15	9.68
Crystallite size at 800 °C (nm)	45.640	21.596	43.157
BET surface area at 600 °C ($m^2\ g^{-1}$)	12.75	23.64	13.85
Crystallite size at 600 °C (nm)	26.958	19.301	20.698

the doped and undoped $Li_{1.03}Mn_{1.97}O_4$. Upon heating to 600 °C, the spinel phase in most of the samples studied showed a spinel phase composition with a relatively consistent small crystallite size, which would change significantly when heated to 850 °C. This implied that the crystallites would start to "fuse" together to form larger crystals at these temperatures.

In summary, the BET surface area and crystallite size parameter of the materials synthesized in the tube furnace at the specific temperatures is also shown and compared in Table II.

The BET results was fairly similar (5.48 $m^2\ g^{-1}$ at 800 °C and 12.75 $m^2\ g^{-1}$ at 600 °C) to those reported by Lee *et al.* (1998) (6.2 $m^2\ g^{-1}$ at 800 °C and 12.2 $m^2\ g^{-1}$ at 600 °C), respectively. These slight changes could be because of the fact that these authors used a different chelating acid together with a slightly higher concentration ratio. It could also be observed that the materials synthesized at higher temperatures produced smaller surface areas and correlates to having higher crystallite sizes (see Table II). The doped oxide materials also produced higher surface areas to the undoped oxide.

IV. CONCLUSION

The study showed that the room temperature precursor materials consisted either of an amorphous phase or a crystalline citrate (Mg–Mn) type phase. Some of the intermediate phases that formed upon heating were shown to either collapse to an amorphous or semi-crystalline Mn_2O_3 phase. Within this study a reasonably pure cathode oxide material was obtained at 400 °C, where the TGA study showed on average, that no other decomposition products formed above this temperature. The results also showed that as the materials that were heated would undergo phase changes up to 400 °C after which the crystallite size and lattice parameter of the formed spinel phase would change with further increase in temperature. Rietveld refinement analysis of the diffraction patterns obtained showed that once the spinel phase of the various materials were formed around 400 °C, the respective unit cells' lattice parameter would increase with increasing temperature up to 800 °C, respectively. In addition, the crystallite size as determined by the Rietveld refined parameter [LVol–IB (nm)], would stay relatively constant up to 600 °C, after which it would increase significantly in value up to 800 °C. This implied that a sintering or conglomeration of the crystallites would start to occur at the synthesis temperature above 600 °C and that ideally, in order to obtain effectively small crystallites of the active material for optimum electrochemical performances, the synthesis temperatures should be kept below 600 °C.

SUPPLEMENTARY MATERIAL

The supplementary material for this article can be found at https://doi.org/10.1017/S088571561600066X.

ACKNOWLEDGEMENTS

The authors thank Nelson Mandela Metropolitan University (NMMU) and the South African National Research Foundation (NRF) for their financial contribution and the University of the Witwatersrand for experimental assistance throughout the study.

Arora, P., Popov, B. N., and White, R. E. (**1998**). "Electrochemical investigations of cobalt-doped $LiMn_2O_4$ as cathode material for lithium-ion batteries," J. Electrochem. Soc. **145**, 807–815.

Bruker, A. X. S. (**2009**). *Topas Manual, Version 4.2 (Computer Software)* (Bruker Software, West Germany).

Chung, K. Y., Ryu, C. W., and Kim, K. B. (**2005**). "Onset mechanism of Jahn-Teller distortion in 4 V $LiMn_2O_4$ and its suppression by $LiM_{0.05}Mn_{1.95}O_4$ (M = Co, Ni) coating," J. Electrochem. Soc. **152**, A791–A795.

Fu, L. J., Liu, H., Li, C., Wu, Y. P., Rahm, E., Holze, R., and Wu, H. Q. (**2005**). "Electrode materials for lithium secondary batteries prepared by sol-gel methods," Progr. Mater. Sci. **50**, 881–928.

Gummow, R. J., de Kock, A., and Thackeray, M. M. (**1994**). "Improved capacity retention in rechargeable 4 V lithium/lithium-manganese oxide (spinel) cells," Solid State Ion. **69**, 59–67.

Guohua, L., Ikuto, H., Uchida, T., and Wakihara, M. (**1996**). "The spinel phases $LiM_yMn_{2-y}O_4$ (M = Co, Cr, Ni) as the cathode for rechargeable lithium batteries," J. Electrochem. Soc. **143**, 178–182.

Hernán, L., Morales, J., Sánchez, L., and Santos, J. (**1999**). "Use of Li-M-Mn-O [M = Co, Cr, Ti] spinels prepared by a sol-gel method as cathodes in high-voltage lithium batteries," Solid State Ion. **118**, 179–185.

Huang, X., Lin, M., Tong, Q., Li, X., Ruan, Y., and Yang, Y. (**2012**). "Synthesis of $LiCoMnO_4$ via a sol-gel method and its application in high power $LiCoMnO_4/Li_4Ti_5O_{12}$ lithium-ion batteries," J. Power Sources **202**, 352–356.

Hwang, B. J., Santhanam, R., and Liu, D. G. (**2001a**). "Characterization of nanoparticles of $LiMn_2O_4$ synthesized by citric acid sol-gel method," J. Power Sources **97**, 443–446.

Hwang, B. J., Santhanam, R., and Liu, D. G. (**2001b**). "Effect of various synthetic parameters on purity of $LiMn_2O_4$ spinel synthesized by sol-gel method at low temperature," J. Power Sources **101**, 86–89.

Jang, D. H., Shin, Y. J., and Oh, S. M. (**1996**). "Dissolution of spinel oxides and capacity losses in 4 V $Li/Li_xMn_2O_4$ cells," J. Electrochem. Soc. **143**, 2204–2211.

Jugovic, D. and Uskokovic, D. (**2009**). "A review of recent developments in the synthesis procedures of lithium iron phosphate powders," J. Power Sources **190**, 538–544.

Kebede, M. A., Phasha, M. J., Kunjuzwa, N., Mathe, M. K., and Ozoemena, K. I. (**2015**). "Solution-combustion synthesized aluminium-doped spinel ($LiAl_xMn_{2-x}O_4$) as a high-performance lithium-ion battery cathode material," Appl. Phys. A **121**, 51–57.

Kim, D. K., Zhang, Y., Voit, W., Rao, K. V., and Muhammed, M. (**2001**). "Synthesis and characterization of surfactant-coated superparamagnetic monodispersed iron oxide nanoparticles," J. Magn. Magn. Mater. **225**, 30–36.

Lee, S. W., Kim, K. S., Moon, H. S., Kim, H. J., Cho, B. W., Cho, W. I., Ju, J. B., and Park, J. W. (**2004**). "Electrochemical characteristics of Al_2O_3-coated lithium manganese spinel as a cathode material for a lithium secondary battery," J. Power Sources **126**, 150–155.

Lee, Y. S., Sun, Y. K., and Nahm, K. S. (**1998**). "Synthesis of spinel $LiMn_2O_4$ cathode material prepared by an adipic acid-assisted sol-gel method for lithium secondary batteries," Solid State Ion. **109**, 285–294.

Li, C., Zhang, H. P., Fu, L. J., Liu, H., Wu, Y. P., Rahm, E., Holze, R., and Wu, H. Q. (**2006**). "Cathode materials modified by surface coating for lithium ion batteries," Electrochim. Acta **51**, 3872–3883.

Li, G., Yamada, A., Fukushima, Y., Yamaura, K., Saito, T., Endo, T., Azuma, H., Sekai, K., and Nishi, Y. (**2000**). "Phase segregation of $Li_xMn_2O_4$ ($0.6 < x < 1$) in non-equilibrium reduction processes," Solid State Ion. **130**, 221–228.

Li, X., Xu, Y. and Wang, C. (**2009**). "Suppression of Jahn-Teller distortion of spinel $LiMn_2O_4$ cathode," J. Alloys Compd. **479**, 310–313.

Liu, H., Wu, Y. P., Rahm, E., Holze, R., and Wu, H. Q. (**2004**). "Cathode materials for lithium ion batteries prepared by sol-gel methods," J. Solid State Electrochem. **8**, 450–466.

Lui, Q., Wang, S., Tan, H., Yang, Z., and Zeng, J. (**2013**). "Preparation and doping mode of doped $LiMn_2O_4$ for Li-ion batteries," Energies **6**, 1718–1730.

Manev, V., Banov, B., Momchiler, A., and Nassalevska, A. (**1995**). "$LiMn_2O_4$ for 4 V lithium-ion batteries," J. Power Sources **57**, 99–103.

Meier, M. (**2004**). *Crystallite Size Measurement Using X-ray Diffraction* (University of California, Davis).

Ohzuku, T., Kitagawa, M., and Hirai, T. (**1990**). "Electrochemistry of manganese dioxide in lithium nonaqueous cell", J. Electrochem. Soc. **137**, 769–775.

Palomares, V., Rojo, T., and Belharouak, I. (eds) (**2012**). *Synthesis Process for Li-ion Battery Electrodes from Solid State Reaction to Solvothermal Self-assembly Methods, in Lithium ion Batteries-New Developments* (InTech, Croatia Europe).

Rehani, B. R., Joshi, P. B., Lad, K. N., and Pratap, A. (**2006**). "Crystallite size estimation of elemental and composite silver nano-powders using XRD principles," Indian J. Pure Appl. Phys. **44**, 157–161.

Rossouw, M. H., de Kock, A., de Picciotto, L. A., Thackeray, M. M., David, W. I. F., and Ibberson, R. M. (**1990**). "Structural aspects of lithium-manganese-oxide electrodes for rechargeable lithium batteries," Mater. Res. Bull. **25**, 173–182.

Seyedahmadian, M., Houshyarazar, S., and Amirshaghaghi, A. (**2013**). "Synthesis and characterization of nanosized spinel $LiMn_2O_4$ via Sol-gel and freeze drying methods," Bull. Korean Chem. Soc. **34**, 622–628.

Singh, P., Sil, A., Nath, M., and Ray, S. (**2010**). "Preparation and characterization of lithium manganese oxide cubic spinel $Li_{1.03}Mn_{1.97}O_4$ doped with Mg and Fe," Physica B **405**, 649–654.

Sun, Y. K. (**1997**). "Synthesis and electrochemical studies of spinel $Li_{1.03}Mn_2O_4$ cathode materials prepared by a sol-gel method for lithium secondary batteries," Solid State Ion. **100**, 115–125.

Sun, Y. K., Oh, I. H., and Kim, K. Y. (**1997**). "Synthesis of spinel $LiMn_2O_4$ by the Sol-Gel method for a cathode-active material in lithium secondary batteries," Ind. Eng. Chem. Res. **36**, 4839–4846.

Sun, Y. K., Kim, D. W., and Choi, Y. M. (**1999**). "Synthesis and characterization of spinel $LiMn_{2-x}Ni_xO_4$ for lithium/polymer battery applications," J. Power Sources **79**, 231–237.

Tarascon, J. M. and Guyomard, D. (**1991**). "Li metal-free rechargeable batteries based on $Li_{1+x}Mn_2O_4$ cathodes ($0 \le x \le 1$) and carbon anodes," J. Electrochem. Soc., **138**, 2864–2868.

Tarascon, J. M. and Guyomard, D. (**1993**). "The $Li_{1+x}Mn_2O_4$/C rocking-chair system: a review," Electrochim. Acta **38**, 1221–1231.

Thackeray, M. M., David, W. I. F., Bruce, P. G., and Goodenough, J. B. (**1983**). "Li-insertion into manganese spinels," Mater. Res. Bull. **18**, 461–472.

Thackeray, M. M., Johnson, P. J., de Picciotto, L. A., Bruce, P. G., and Goodenough, J. B. (**1984**). "Electrochemical extraction of lithium from $LiMn_2O_4$," Mater. Res. Bull. **19**, 179–187.

Thackeray, M. M., de Kock, A., Rossouw, M. H., Liles, D. C., Hoge, D., and Bittihn, R. (**1992**). "Spinel electrodes from the Li-Mn-O system for rechargeable lithium battery applications," J. Electrochem. Soc. **139**, 363–366.

Thirunakaran, R., Sivashanmugam, A., Gopukumar, S., Dunnill, C. W., and Gregory, D. H. (**2008**). "Studies on chromium/aluminium-doped manganese spinel as cathode materials for lithium-ion batteries-A novel chelated sol-gel synthesis," J. Mater. Process. Technol. **208**, 520–531.

Wang, J. L., Li, Z. H., Yang, J., Tang, J. J., Yu, J. J., Nie, W. B., Lei, G. T., and Xiao, Q. Z. (**2012**). "Effect of Al-doping on the electrochemical properties of a three-dimensionally porous lithium manganese oxide for lithium-ion batteries," Electrochim. Acta **75**, 115–122.

Wang, X., Chen, X., Gao, L., Zheng, H., Shen, M. I. T., and Zhang, Z. (**2003**). "Citric acid-assisted sol-gel synthesis of nanocrystalline $LiMn_2O_4$ spinel as cathode material," J. Cryst. Growth **256**, 123–127.

Wu, S. and Chen, H. (**2003**). "The effects of heat-treatment temperature on the retention capacities of spinels prepared by the Pechini process," J. Power Sources **119–121**, 134–138.

Yamada, A. (**1996**). "Lattice instability in $Li(Li_xMn_{2-x})O_4$," J. Solid State Chem. **122**, 160–165.

Yi, T., Dai, C., Gao, K., and Hu, X. (**2006a**). "Effects of synthetic parameters on structure and electrochemical performance of spinel lithium manganese oxide by citric acid-assisted sol-gel method," J. Alloys Compd. **425**, 343–347.

Yi, T., Hu, X., and Gao, K. (**2006b**). "Synthesis and physicochemical properties of $LiAl_{0.05}Mn_{1.95}O_4$ cathode material by ultrasonic-assisted sol-gel method," J. Power Sources **162**, 636–643.

Zhong, Q., Bonakdarpour, A., Zhang, M., Gao, Y., and Dahn, J. R. (**1997**). "Synthesis and electrochemistry of $LiNi_xMn_{2-x}O_4$," J. Electrochem. Soc. **144**, 205–213.

https://doi.org/10.1017/S088571561600066X Published online by Cambridge University Press